Chinese Chemical Letters 36 (2025) 110395

Contents lists available at ScienceDirect

Chinese Chemical Letters

journal homepage: www.elsevier.com/locate/cclet

Design and fabrication of triangle-pattern superwettability hybrid surface with high-efficiency condensation heat transfer performance

Rui Wang[a,1], Yuan Tian[a,1], Xuefeng Gao[a,b,*], Lei Jiang[c]

[a] Suzhou Institute of Nano-Tech and Nano-Bionics, Chinese Academy of Sciences, Suzhou 215123, China
[b] School of Nano-Tech and Nano-Bionics, University of Science and Technology of China, Hefei 230026, China
[c] Technical Institute of Physics and Chemistry, Chinese Academy of Sciences, Beijing 100190, China

ARTICLE INFO

Article history:
Received 20 May 2024
Revised 27 August 2024
Accepted 30 August 2024
Available online 31 August 2024

Keywords:
Superwettability
Hybrid surface
Superhydrophobic
Superhydrophilic
Patterned surfaces
Condensation heat transfer

ABSTRACT

Utilizing superwettability micro/nanostructures to enhance the condensation heat transfer (CHT) performance of engineering materials has attracted great interest due to its values in basic research and technological innovations. Currently, exploring facile micro/nanofabrication approaches to create high-efficiency CHT surfaces has been one of research hotspots. In this work, we propose and demonstrate a type of new superwettability hybrid surface for high-efficiency CHT, which consists of superhydrophobic nanoneedle arrays and triangularly-patterned superhydrophilic microdots (SMDs). Such hybrid surface can be fabricated by the facile growth of densely-packed ZnO nanoneedles on the Zn-electroplated copper surface followed by fluorosilane modification and mask-assisted photodegradation. Through regulating the diameters and interspaces of SMDs, we obtain the optimized triangularly-patterned hybrid surface, which shows 42.7% higher CHT coefficient than the squarely-patterned hybrid surface and 58.5% higher CHT coefficient than the superhydrophobic surface. The key of such hybrid surface design is to considerably increase CHT coefficient brought about by SMD-triggered drop sweeping at the cost of slightly reducing heat transfer area of superhydrophobic functional zone for drop jumping. Such new strategy helps develop advanced CHT surfaces for high-efficiency electronic cooling and energy utilization.

Condensation is ubiquitous in nature and has been widely used in electronic cooling devices such as vapor chambers and heat pipes for removing waste heat generated by chip running [1-3]. Along with the advance of micro/nanofabrication technologies and bionic superwettability surface systems [4-10], great interest has been focused on exploring superwettability surface designs and their fabrication technologies that can improve the condensation heat transfer (CHT) performance of engineering materials [8-28]. An ideal CHT interface requires lower nucleation energy barrier, more nucleation sites for phase-change energy exchange, smaller departure sizes for reducing the thermal resistance of condensate drops and quicker renewal [8-10]. These properties have inherent conflicting requirements to either hydrophilicity or hydrophobicity, which can be realized by rationally designing superhydrophobic hybrid surfaces with microscopic wettability contrast [26-29]. Latest researches demonstrate that, compared with low-adhesive superhydrophobic surfaces with jumping function of condensate microdrop, superwettability hybrid surfaces with square-patterned hydrophilic microdots have apparently higher CHT coefficient [26-28]. Drops condensed at these microdots can self-remove *via* the coalescence-induced jumping or sweeping way, depending on their interface adhesion. As compared to jumping drops, sweeping drops have larger resident sizes, higher thermal resistance and slower renewal, all of which are adverse to CHT. Interestingly, a sweeping event can remove tens of, hundreds of and even more drops along the way, which depends on the size and distance of sweeping drops, while a jumping event only can remove several tiny drops. Therefore, rationally-designed superwettability hybrid surfaces exhibit higher CHT coefficient than superhydrophobic surfaces. However, all these innovative researches take a square pattern of hydrophilic microdots [26-28].

To our knowledge, superhydrophilic microdots (SMDs) with composite heat conduction paths are preferrable to creating the superwettability hybrid surface since they have smaller interface thermal resistance than hydrophilic microdots. Besides, rationally-designed triangle pattern with dislocation-arranged SMDs can remove more surface regions of tiny condensate drops *via* the drop sweeping (Fig. S1 in Supporting information) and consequently dynamically expose more bare sites for energy exchange than the

* Corresponding author.
E-mail address: xfgao2007@sinano.ac.cn (X. Gao).
[1] These authors contributed equally to this work.

https://doi.org/10.1016/j.cclet.2024.110395
1001-8417/

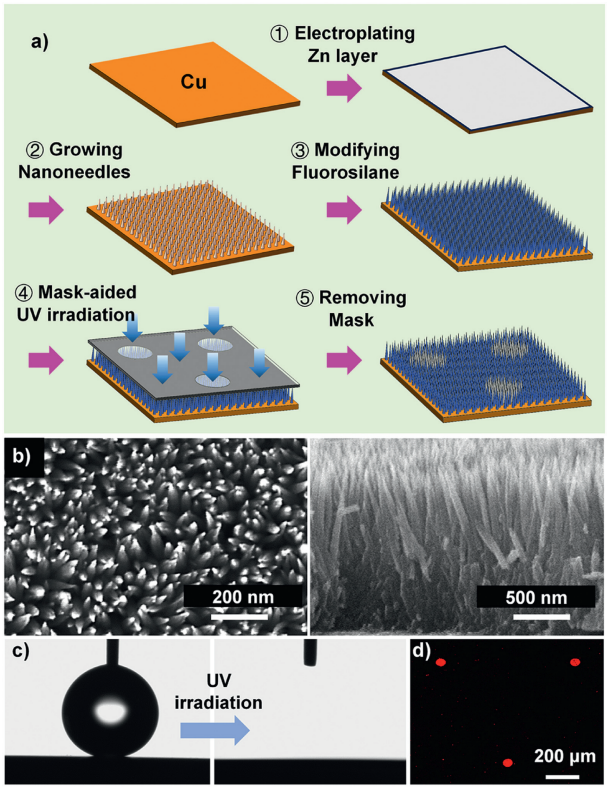

Fig. 1. (a) A schematic presenting the fabrication flow chart of superwettability hybrid surface with triangularly-patterned SMDs. (b) SEM top-view (left) and side-view (right) of as-prepared ZnO nanoneedles. (c) Optical images showing that the superhydrophobic state (left) of the silane-modified nanoneedle surface can switch into the superhydrophilic state (right) after UV irradiation. Here, the tested water drop is 4 μL. (d) Fluorescence image of triangularly-patterned SMDs with diameter of 40 μm and interspace of 800 μm.

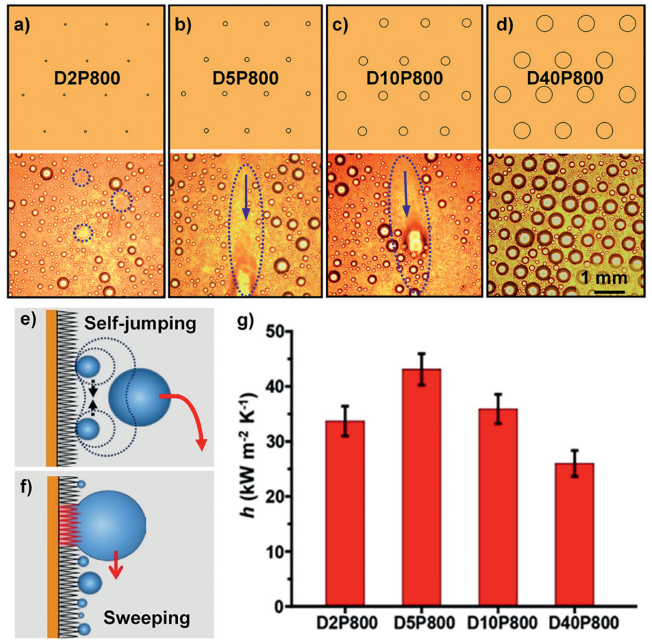

Fig. 2. Schematics (top) and condensation behaviours (bottom) of triangularly-patterned superwettability hybrid surfaces with varied SMD diameters: (a) $D = 2$ μm, (b) 5 μm, (c) 10 μm and (d) 40 μm. Their interspaces are fixed as 800 μm. Snapshots showing their difference in condensation mass transfer ability (Movie S1). Drop sweeping events are denoted by oval blue dotted lines, while the arrows reflect the sweeping direction of drops. Out-of-plane jumping events are denoted by circular dotted lines. (e) Schematic shows self-removal of condensate drops on the superhydrophobic functional zones in the out-of-plane self-jumping way, driven *via* coalescence-released surface energy. (f) Schematic shows sweeping of a big condensate drop at the SMD site, which can remove a large number of drops along the way. (g) Histogram showing measured CHT coefficients of these four hybrid samples. Clearly, CHT coefficient first increases and then decreases with the increase of SMD diameter, where D5P800 has the best performance.

square pattern with aligned hydrophilic microdots. However, such new hybrid surface with triangle-pattern SMDs has not been reported for CHT to date.

We propose and demonstrate that well-designed triangle-pattern superwettability hybrid surface, which is fabricated by the facile growth of ZnO nanoneedles followed by silane modification and mask-aided photodegradation, has much higher CHT coefficient than the square-pattern hybrid surface and the superhydrophobic surface. Such new superwettability hybrid surface design strategy is simple and effective in enhancing CHT.

Fig. 1a shows the fabrication flow chart of superwettability hybrid surface with triangle-pattern SMDs. This approach includes five steps. First, the copper surface is electroplated with a thin Zn layer, which is implemented in an aqueous solution of 0.1 mol/L KCl and 0.2 mmol/L $ZnCl_2$ for 5 min at −1.8 V. Second, ZnO nanoneedles are grown on the Zn-electroplated copper surface in an aqueous solution of 0.25 mol/L $Zn(NO_3)_2{\cdot}6H_2O$ and 2 mol/L NaOH at 60 °C for 30 min. Third, the nanoneedle surface is modified by a classical vapor phase single-layer silane self-assembly process, where samples are placed together with a cup containing 10 μL 1*H*,1*H*,2*H*,2*H*-perfluorodecyltrimethoxysilane liquid into a glass container (Φ145 mm × 70 mm) and the container is sealed with a cap and then heated for 2 h at 120 °C. Fourth, SMDs can generate on the silane-modified nanoneedle surface by mask-aided photodegradation. Finally, desired superwettability hybrid surfaces can be obtained after removing the mask. Diameters, interspaces and arrangement ways of SMDs can be governed by the masks. Clearly, all these processing steps are not only simple but readily implemented in a common chemistry or material lab.

Fig. 1b first shows SEM top-view (left) and side-view (right) of ZnO nanoneedles. It is evident that these aligned nanoneedles appear very dense, which density reaches 2.2×10^8 mm^{-2}. Their average tip diameter and height are 10 nm and 2.1 μm respectively. The surface of ZnO nanoneedle arrays becomes superhydrophobic after silane modification and is switched into superhydrophilicity *via* ultraviolet (UV) irradiation (Fig. 1c). ZnO is a type of photocatalyst, which can degrade fluorosilane molecules of nanoneedle surface [30]. Our study proves that such SMD pattern cannot be visualized by usual imaging technologies such as optical and scanning electron microscopies. To intuitively present SMD patterns formed by mask-aided photodegradation, a fluorescence-imaging technique based on rhodamine B labeling is used here [30]. Rhodamine B labelled SMD patterns can be imaged by confocal laser microscope. Details about the sample fabrication can be found in Supporting information. Fig. 1d shows the fluorescence image of an exemplified triangle-pattern superwettability hybrid surface. The diameter and interspace of SMDs are 40 μm and 800 μm, respectively. Clearly, our used method can tailor any desired SMD patterns, which diameters, interspaces and arrangement ways can be facilely governed by the masks.

To optimize the CHT property of the triangularly-patterned superwettability hybrid surface, we first explore the influence of SMD diameters (D) in the case of fixing the interspace ($P = 800$ μm). Figs. 2a-d show the schematics (top) and condensation behaviours (bottom) of the hybrid samples with $D = 2$ μm, 5 μm, 10 μm and 40 μm. Details about their condensation mass transfer ability differences can be found in Movie S1 (Supporting information). Through microscopic optical imaging, we can identify three kinds of conden-

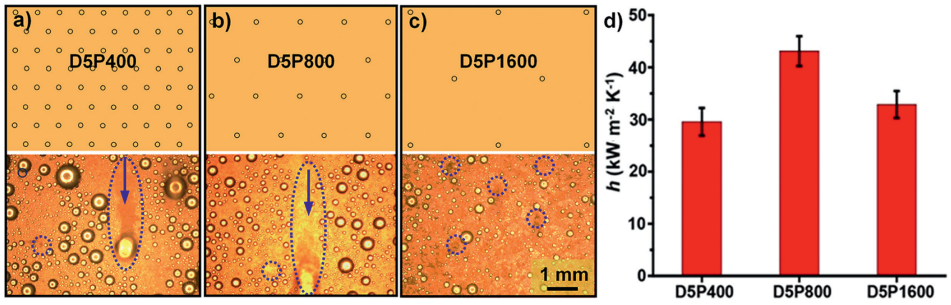

Fig. 3. Schematics (top) and condensation behaviours (bottom) of triangularly-patterned superwettability hybrid surfaces with varied SMD interspaces: (a) $P = 400\,\mu m$, (b) $800\,\mu m$, and (c) $1600\,\mu m$. Their diameters are fixed as $5\,\mu m$. Snapshots showing their difference in condensation mass transfer ability (details see Movie S2). Drop sweeping events are denoted by oval blue dotted lines, while the arrows reflect the sweeping direction of drops. Out-of-plane jumping events are denoted by circular dotted lines. (d) Histogram showing measured CHT coefficients of these three hybrid samples. Clearly, sample D5P800 is the optimal, which performance becomes worse as the interspace of SMDs decreases to $400\,\mu m$ or increases to $1600\,\mu m$.

sation behaviours: (1) The drop jumping and sweeping events coexist on all sample surfaces; (2) more large drops can reside on the sample surface along with the increase of SMD diameter; and (3) the mobile ability of condensate drops at the SMDs can be severely inhibited as D up to $40\,\mu m$. It is well-known that, in real vapor chamber for CHT characterization, it is hard to clearly capture the microscopic details of the drop coalescence-triggered jumping and sweeping due to the limitation of high-resolution optical imaging ability. To facilitate reader's understanding, we provide schematics of the drop jumping (Fig. 2e) and sweeping (Fig. 2f), which occur on the superhydrophobic functional zones and SMD sites, respectively. Note that the drop sweeping events also occur at some defects that are uncontrollable and inevitable during wet-chemistry growth process. Fig. 2g gives the measured CHT coefficients (h) of these four hybrid surfaces. Here, the tested vapor temperature, vapor pressure and surface subcooling are 40 °C, 7.38 kPa and 2 K, respectively. As the fluctuation of vapor temperature is below 0.5 °C, the steady-state test condition is reached and then 120 data points are collected within 2 min. Details about CHT performance characterization can be found in Supporting information. Evidently, CHT coefficient can first increase and then decrease along with the increase of D, where sample D5P800 is the optimal. The tested CHT coefficients of D2P800, D5P800, D10P800 and D40P800 are 33.7, 43.1, 35.9 and 25.9 kW m^{-2} K^{-1}, corresponding heat fluxes are 67.4, 86.2, 71.8 and 51.8 kW/m^2. How to understand their variation trend? Firstly, total CHT coefficient can be considered as the sum of CHT coefficients of the drop jumping (h_j) and sweeping (h_s). Among other, h_j value gradually decreases along with the increase of D since bigger SMDs result in less superhydrophobic area for drop jumping. Accordingly, the "first increase and then decrease" variation trend of h values should be ascribed to the samples' difference in the h_s value. No doubt that properly increasing D is beneficial to CHT because relatively bigger mobile drops initiated at the SMDs can take away more tiny drops along the way. However, too large SMDs have too strong solid-liquid interface adhesion. This would result in the great delay and even complete inhibition of sweeping initiation, which is adverse to CHT. It is the cooperation of the positive and negative effects that results in the first increase and then decrease of h_s (and h) along with the increase of D. Here, $D = 5\,\mu m$ is the optimal.

Subsequently, we explore the influence of SMD interspaces to the performance of the triangularly-patterned hybrid surface. Figs. 3a–c exhibit schematics (top) and condensation behaviours (bottom) of samples with $P = 400\,\mu m$, $800\,\mu m$ and $1600\,\mu m$ in the case of fixing $D = 5\,\mu m$. Details about their condensation mass transfer capability differences can be found in Movie S2 (Supporting information). Fig. 3d shows their CHT coefficients. CHT coefficients of D5P400, D5P800 and D5P1600 are 29.5, 43.1 and 32.9 kW m^{-2} K^{-1}, corresponding heat fluxes are 59.0, 86.2 and 65.8 kW/m^2. Clearly, sample D5P800 is the optimal, which performance becomes worse as the interspace of SMDs decreases to $400\,\mu m$ or increases to $1600\,\mu m$. Among others, the property of D5P400 appears the worst. Compared with D5P800, D5P400 has much more SMDs. This decreases the heat transfer area of superhydrophobic zone available for drop jumping and increases the mobile resistance of drops during their sweeping processes. As a result, the h_j and h_s components are reduced. This is why the performance of D5P400 is inferior to that of D5P800. In sharp contrast, the number of SMDs will dramatically decrease as their interspace increases from $800\,\mu m$ up to $1600\,\mu m$. This increases more areas of superhydrophobic surface for CHT for the drop jumping, which is beneficial to increasing h_j. However, the dramatical decrease of SMD number can decrease the number of sweeping drops, which is adverse to timely removal of condensate drops on the whole hybrid surface. The h_s component would be greatly reduced. We can reasonably infer that the latter negative effect is stronger to CHT than the former positive effect. This is the reason why CHT performance of D5P1600 is inferior to that of D5P800. In this case, $P = 800\,\mu m$ is the optimal.

To highlight the advantage of triangle-pattern superwettability hybrid surface design in enhancing CHT, we also fabricate square-pattern superwettability hybrid surface with fully identical SMD diameters ($5\,\mu m$) and interspaces ($800\,\mu m$) and superhydrophobic surface without SMDs. Figs. 4a-c show their schematics (top) and condensation behaviours (bottom). Details about the condensation mass transfer ability differences can be found in Movie S3 (Supporting information). Fig. 4d shows the CHT coefficients of these three samples. CHT coefficients of superhydrophobic surface with the optimal triangle pattern, with the contrast square pattern and without patterned SMDs are 43.1, 30.3 and 27.4 kW m^{-2} K^{-1}, corresponding heat fluxes are 86.2, 60.6 and 54.8 kW/m^2. Clearly, the properties of these two hybrid surfaces are superior to that of the superhydrophobic surface. Among others, the triangle-pattern hybrid surface outperforms the square-pattern hybrid surface. The optimal triangle-pattern hybrid surface shows 42.7% higher CHT coefficient than square-pattern surface and 58.5% higher CHT coefficient than superhydrophobic surface, respectively. It should be pointed out that the triangle pattern has higher SMD density than the square pattern as fixing D and P. It is well-known that SMD regions has apparently lower CHT efficiency than superhydrophobic regions [11-29]. That is, introducing the triangle pattern on the superhydrophobic surface should have lower total CHT coefficient than the square pattern. However, our study demonstrates that the triangle pattern can achieve apparently higher total CHT coefficient than the square pattern (Fig. 4d). Such CHT enhancement can be ascribed to sweeping-enhanced drop removal brought about by the

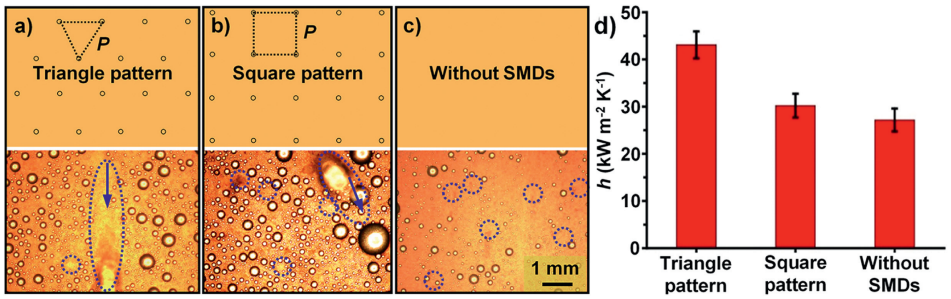

Fig. 4. Schematics (top) and condensation behaviours (bottom) of superhydrophobic surfaces with the triangle-patterned SMDs (a), with the square-patterned SMDs (b) and without SMDs (c). Two SMD patterns have the same diameters (5 μm) and interspaces (800 μm). Snapshots showing their difference in condensation mass transfer ability (Movie S3). Drop sweeping events are denoted by oval blue dotted lines, while the arrows reflect the sweeping direction of drops. Out-of-plane jumping events are denoted by circular dotted lines. (d) Histogram showing CHT coefficients of these three samples. Clearly, CHT performance of two hybrid surfaces are superior to that of the superhydrophobic surface and the triangle pattern outperforms the square pattern. The triangle-pattern surface shows 58.5% higher CHT coefficient than the superhydrophobic surface.

triangle-patterned SMDs (Fig. S2 in Supporting information). In this case, the triangle pattern with higher SMD density and more rational spatial layout can make sweeping drops remove more surface regions of tiny drops along the way than the square patten. More regions of drops are timely removed, which exposes more bare sites for new nucleation and energy exchange. Thus, the triangle pattern has much higher CHT coefficient than the square pattern. Here, a specific pattern has a specific SMD density. "SMD density" is the intrinsic result of "the specific pattern", where the former is governed by the latter. CHT enhancement can be considered as the contribution from increased SMD density in the case of comparing the triangle pattern (Fig. 4a) with the square pattern (Fig. 4b), but this concept is not necessarily true in other cases. For example, compared with D5P800, D5P400 with much higher SMD density has much lower CHT coefficient. Accordingly, such understanding "CHT enhancement results from more rational spatial layout of the triangle-pattern rather than its increased SMD density" is more accurate for all cases in this work. The key of such hybrid surface design is to considerably increase the CHT coefficient brought about by enhanced drop sweeping at the cost of slightly reducing heat transfer area of superhydrophobic zone for drop jumping. As compared to the superhydrophobic surface without SMDs, the optimal triangle-pattern hybrid surface can greatly increase the h_s component at the cost of properly reducing the h_j component. Therefore, the triangle pattern design is more suitable for creating superwettability hybrid surface to achieve more efficient CHT.

In conclusion, we develop a type of new superwettability hybrid surface with high-efficiency CHT performance and demonstrate that rationally-designed triangle pattern is superior to square pattern. By tuning the diameters and interspaces of SMDs, we can obtain the optimal triangle-pattern superwettability hybrid surface. The key of such hybrid surface design is to considerably increase CHT coefficient brought about by enhanced drop sweeping at the cost of slightly reducing heat transfer area of superhydrophobic zone for drop jumping. This new hybrid surface design strategy of utilizing the triangle-pattern SMDs to enhance the CHT performance helps develop advanced CHT interfaces for high-efficiency electronic cooling and energy utilization. Besides, our preliminary study has demonstrated that using microcavities to replace SMDs of the triangle-pattern surface likewise can induce the drop sweeping and exhibit almost identical property (Fig. S3 in Supporting information). Based on this work, further regulating different profiles of SMDs and their orientations, any two side lengths of triangle-patterns and their intersection angles would help provide new insights into superwettability hybrid surface designs so as to obtain more efficient CHT, which is not only of fundamental scientific significance, but also helps develop advanced CHT interfaces for technological applications. In the near future, more studies need be carried out to assess the effectiveness of these superwettability hybrid surfaces in vapor-liquid phase change cooling devices.

Declaration of competing interest

The authors declare that they have no known competing financial interests or personal relationships that could have appeared to influence the work reported in this paper.

CRediT authorship contribution statement

Rui Wang: Visualization, Investigation. **Yuan Tian:** Writing – review & editing, Writing – original draft. **Xuefeng Gao:** Writing – review & editing, Supervision, Conceptualization. **Lei Jiang:** Writing – review & editing.

Acknowledgments

This work was supported by National Natural Science Foundation of China (No. 21573276), Natural Science Foundation of Jiangsu Province (No. BK20170007) and Jiangsu Funding Program for Excellent Postdoctoral Talent (No. 2022ZB846). We thank Peiyu Lv and Qiulong Tang for their help in making Fig. 1a and editing Movies S1-S3, respectively.

Supplementary materials

Supplementary material associated with this article can be found, in the online version, at doi:10.1016/j.cclet.2024.110395.

References

[1] X. Ji, J. Xu, H. Li, G. Huang, Nano Energy 38 (2017) 313–325.
[2] H. Tang, Y. Tang, Z. Wan, et al., Appl. Energy 223 (2018) 383–400.
[3] J.L. Luo, D.C. Mo, Y.Q. Wang, S.S. Lyu, ACS Nano 15 (2021) 6614–6621.
[4] M. Liu, S. Wang, L. Jiang, Nat. Rev. Mater. 2 (2017) 17036.
[5] Y. Wang, J. Li, Z. Shang, et al., Chin. Chem. Lett. 35 (2024) 109623.
[6] Q. Wu, Y. Cui, G. Xia, et al., Chin. Chem. Lett. 35 (2024) 108687.
[7] J. Zhao, S. Wang, S. Zhao, et al., Chin. Chem. Lett. 36 (2025) 109883.
[8] H.J. Cho, D.J. Preston, Y. Zhu, E.N. Wang, Nat. Rev. Mater. 2 (2016) 16092.
[9] X. Gong, X. Gao, L. Jiang, Adv. Mater. 29 (2017) 1703002.
[10] R. Wen, X. Ma, Y.C. Lee, R. Yang, Joule 2 (2018) 2307–2347.
[11] N. Miljkovic, R. Enright, Y. Nam, et al., Nano Lett. 13 (2013) 179–187.
[12] J. Zhu, Y. Luo, J. Tian, J. Li, X. Gao, ACS Appl. Mater. Interfaces 7 (2015) 10660–10665.
[13] R. Wen, Q. Lia, J. Wu, et al., Nano Energy 33 (2017) 177–183.
[14] R. Wang, J. Zhu, K. Meng, et al., Adv. Funct. Mater. 28 (2018) 1800634.
[15] R. Wen, S. Xu, X. Ma, Y.C. Lee, R. Yang, Joule 2 (2018) 269–279.
[16] C.S. Sharma, C. Stamatopoulos, R. Suter, P.R. Rohr, D. Poulikakos, ACS Appl. Mater. Interfaces 10 (2018) 29127–29135.
[17] R. Wen, S. Xu, D. Zhao, et al., Natl. Sci. Rev. 5 (2018) 878–887.
[18] Q. Peng, L. Jia, J. Guo, et al., Appl. Phys. Lett. 114 (2019) 133106.
[19] C.W. Lo, Y.C. Chu, M.H. Yen, M.C. Lu, Joule 3 (2019) 2806–2823.

[20] R. Wang, F. Wu, D. Xing, F. Yu, X. Gao, ACS Appl. Mater. Interfaces 12 (2020) 24512–24520.
[21] S. Chen, R. Wang, F. Wu, et al., Mater. Today Phys. 19 (2021) 100407.
[22] Y. Tang, X. Yang, Y. Li, Y. Lu, D. Zhu, Nano Lett. 21 (2021) 9824–9833.
[23] L. Zhou, W. He, M. Wang, X. Hou, ChemSusChem 15 (2022) e202102531.
[24] L. Shan, Z. Guo, D. Monga, D. Boylan, X. Dai, Joule 7 (2023) 168–182.
[25] Y.C. Zhang, T.Y. Zhang, L.W. Fan, Adv. Funct. Mater. 33 (2023) 2305029.
[26] Y. Hou, M. Yu, X. Chen, Z. Wang, S. Yao, ACS Nano 9 (2015) 71–81.
[27] J. Xie, J. Xu, Q. Liu, X. Li, Adv. Mater. Interfaces 4 (2017) 1700684.
[28] Z. Song, M. Lu, X. Chen, ACS Omega 5 (2020) 23588–23595.
[29] Y. Tang, X. Yang, L. Wang, Y. Li, D. Zhu, ACS Appl. Mater. Interfaces 15 (2023) 21549–21561.
[30] D. Xing, R. Wang, F. Wu, X. Gao, ACS Appl. Mater. Interfaces 12 (2020) 29946–29952.